Landslides (2019) 16:283–293
DOI 10.1007/s10346-018-1066-1
Received: 23 January 2018
Accepted: 25 September 2018
Published online: 6 November 2018

Weiyuan Zhang · Amin Askarinejad

Behaviour of buried pipes in unstable sandy slopes

Abstract Significant forces can be applied to embedded pipelines in sloping grounds due to soil instabilities, which potentially might lead to leakage of hazardous fluids into the environment. The soil-pipeline interaction in sandy slopes has been investigated experimentally using small-scale physical models tested in geotechnical centrifuge. A novel method is developed in this paper to estimate the ultimate external forces, induced by slope failures, acting on buried pipes at various locations inside the slope. Instabilities were triggered by surcharge loading on the slope crest in the centrifuge tests. Six dense coarse sandy slopes were tested with different pipe locations with respect to the slope crest. Moreover, two medium dense fine sand slopes were tested in the same manner to study the effect of the grain size distribution on the soil-pipe interaction. The external forces on the pipe induced by the surrounding soil movements were calculated based on the measurements of four strain gauges installed on the pipe. The shape of failure surface and pipe movements were monitored with the aid of advanced image analysis techniques. The results indicate that a buried pipeline has the potential to affect the slope failure mechanism. Normalised force-pipe displacement relationships were derived and compared to the estimation methods suggested in previous studies, which were mainly done on pipes installed in flat grounds. A new prediction method is introduced in this study, which considers the pipe burial distance to the slope crest. Moreover, the slope angle effect on the ultimate force applied to the pipe is also investigated, and a generalised formula is developed. Finally, two examples of the application of the new method are presented for pipelines installed at the toe of two large-scale subarial and submarine slopes.

Keywords Slope pipeline interaction · Physical modelling · Image analysis · Landslide · Pipeline

Introduction

Pipelines are widely used to transport fluids over long distances and may pass through various geological and topographic conditions. Due to the environmental and safety concerns or constraints imposed by the land use, pipelines are sometimes placed in sloping grounds in either onshore or offshore projects. However, relative movements of the soil and the pipe can impose major external loads to the structure, which might eventually result in the failure of pipelines along unstable slopes. It is reported that ground movement, such as slope instability, was the reason of 13% of European gas pipeline incidents during the period from 2004 to 2013 (Wu et al. 2017). The acting forces induced by soil movements have direct relationship with the relative soil-pipe movement (Chan and Wong 2004; Feng et al. 2015; Rammah et al. 2014), and are categorised as one of the major threats to the pipeline operation. Therefore, reliable perdition of the external forces applied to the pipe as a result of slope instability is of utmost importance in the design or evaluation process. Moreover, the relationship between the peak external load and the corresponding pipe displacement as well as the determination of the corresponding structural stresses or strains are necessary for a safe design of pipelines buried in slopes.

During a slope or an embankment instability, an embedded pipe might move along a curved path with horizontal, vertical and/or longitudinal components (Fig. 1a). Di Prisco and Galli (2006) indicated that the vertical and horizontal soil resistance have coupling effects. However, physical modelling of the soil-pipeline interaction is traditionally conducted by pulling or pushing the pipeline horizontally in level grounds using wires or rigid shafts along a constant direction (Fig. 1b) (Audibert and Nyman 1977; Trautmann and O'Rourke 1985; Paulin 1998; Calvetti et al. 2004; Liu et al. 2015; Sahdi et al. 2014; Almahakeri et al. 2013; Ono et al. 2017; Roy and Hawlader 2012; Zhang et al. 2002; Oliveira et al. 2009; Tian and Cassidy 2011). Ignoring the direction of the pipe movement might result in an underestimation of the loads that the soil can exert on the pipe (Calvetti et al. 2004).

Physical modelling of the soil–pipe interaction

Based on the results of small-scale tests on buried pipes pulled horizontally under a flat soil surface, Audibert and Nyman (1977) suggested that the ultimate soil resistance (q_u) is expressed as follows:

$$q_u = \gamma H_c N_{uq} = F_{ud}/DL \tag{1}$$

where γ is the soil unit weight; H_c is the pipe embedment depth (from the soil surface to the centre of the pipe); N_{uq} is the ultimate bearing capacity factor proposed by Hansen (1961), which is also known as the ultimate dimensionless force; F_{ud} is the maximum drag force applied on the pipe; D and L are the pipe diameter and pipe length, respectively. Liu et al. (2015) designed lateral pull-out tests to investigate the resultant forces on the pipelines both in sand and soft clay samples. They claimed that the lateral soil resistance increases with increasing embedment ratio, H_c/D. Oliveira et al. (2017) studied the lateral soil movement-pipe interaction in centrifuge condition using a marine soil (soil internal friction angles, $\phi' = 24.8°$). The soil movements were developed by moving a plate, which was partially embedded into the clay samples towards the buried pipe. They observed that the induced force rises slightly as the embedment ratio increases.

Audibert and Nyman (1977) found that the normalised force-displacement relationship of a pipe pulled horizontally below a flat soil surface can be fitted by means of a hyperbolic curve as expressed by the following:

$$\frac{F_d}{F_{ud}} = \frac{{}^{y}/_{y_u}}{a + b\,{}^{y}/_{y_u}} \tag{2}$$

where F_d is the drag force, y is the pipe movement, y_u is the pipe movement corresponding to F_{ud}, a and b are two model constants.

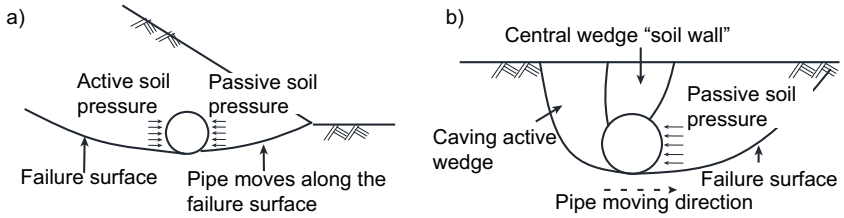

Fig. 1 Failure mechanism: a) a pipe buried within a slope; b) a pipe pulled horizontally in a flat ground

Table 1 Scaling laws for centrifuge model tests

Parameters	Unit	Model/prototype
Acceleration	m/s^2	N
Dimensions (length, diameter, thickness)	m	1/N
Pipe external force (F_N)	kN/m	1/N
Pipe flexural rigidity (EI) *	kN·m	$1/N^3$
Pipe cross-section outer strain (ε)	–	1
Bearing capacity factor (N_q)	–	1

*I is the second moment of area per unit length

Based on results from both loose and dense samples (ϕ' is 33° and 40°, respectively, reported by Trautmann and O'Rourke (1985)), Audibert and Nyman (1977) found that all the results fell into a region bounded by an upper ($a = 0.0486$, $b = 0.9554$), and a lower ($a = 0.2405$, $b = 0.7566$) hyperbolic curves. Trautmann and O'Rourke (1985) fitted their test results using $a = 0.17$ and $b = 0.83$. Yimsiri et al. (2004) suggested $a = 0.1$ and $b = 0.9$ for deep-buried pipes in medium dense sand with H_c/D ranging from 11.5 to 100.

Trautmann and O'Rourke (1985) performed large-scale pipe pulling tests in a container with dimensions of 2.3 (length) × 1.2 (width) × 1.2 (depth) m^3 and discovered that N_{uq} increases linearly with H_c/D when H_c/D is less than eight. Hsu (1996) studied the soil restraint on pipelines, which were pulled with various oblique angles with respect to the horizontal plane. They observed that N_{uq} decreases with the increase of the oblique angle, prominently when the oblique angle is within 45°. This observation is in agreement with the prediction of Nyman (1984), who extended the inclined anchor-soil behaviour to the buried pipe-soil behaviour.

Based on the results of the tests on pipes which were pulled at an inclination of 30° with respect to the horizontal direction in loose sand samples with $\phi' = 33°$, Hsu (1996) reported that the value of y_u is equal to 0.075 H_c and 0.085 H_c for $H_c/D = 3.5$ and 1.5, respectively. Trautmann and O'Rourke (1985) suggested that the pipe displacement at the ultimate soil resistance y_u, the ultimate displacement, can be estimated as follows:

$$\begin{cases} y_u = 0.13\, H_c \left(\text{for loose sand}, \phi' = 31^\circ\right) \\ y_u = 0.08\, H_c \left(\text{for medium dense sand}, \phi' = 36^\circ\right) \\ y_u = 0.03\, H_c \left(\text{for dense sand}, \phi' = 44^\circ\right) \end{cases} \quad (3)$$

The majority of the experimental work conducted to study the soil-pipeline interaction is performed on small or medium scale models at normal Earth gravity condition (1 g). This type of physical modelling technique, although quite informative in a qualitative way, cannot be used reliably for quantitative analysis as the stress state of the soil in the model and prototype are different (Terzaghi 1943). An alternative to this technique is the use of geotechnical centrifuge. In the centrifuge tests a model with geometry of N times smaller than the prototype is constructed and is tested under enhanced acceleration field with a magnitude of N times the Earth's gravity (Ng). This situation provides a gradient of body stresses within the model similar to the prototype, which ensures similar effective stresses and pore pressures at equivalent depths (Wood 2003; Schofield 1980; Taylor 1995). The prototype behaviour is approximated in

Table 2 Geotechnical characteristics of Delft Centrifuge Sand and Geba Sand

Property	DC Sand	Geba Sand
D_{10}, D_{30}, D_{50}, D_{60} (mm)	0.74, 0.85, 0.92, 0.98	0.078, 0.110, 0.117, 0.121
Specific gravity, G_s (–)	2.65	2.67
Minimum void ratio (–)	0.52	0.64
Maximum void ratio (–)	0.72	1.07
Residual friction angle (°)	33.6	36.0

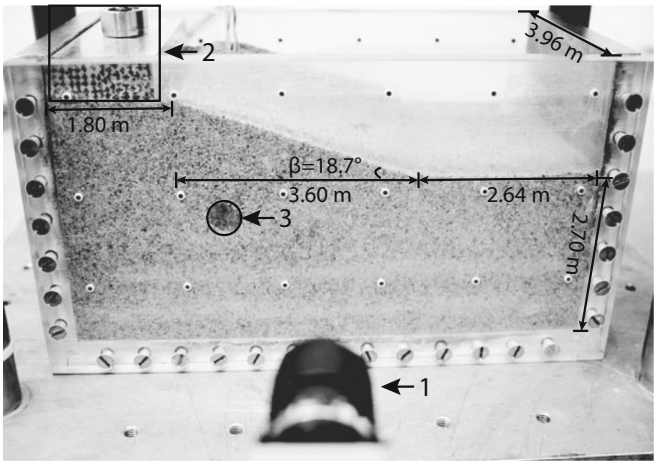

Fig. 2 Test set-up: (1) high-resolution digital camera; (2) load cell and footing; (3) instrumented pipe (dimensions in prototype scale)

accordance with scaling laws in the centrifuge model testing. The major scaling laws are summarised in Table 1.

This paper presents the results of a series of centrifuge model tests with pipes buried in unstable dense sandy slopes. Slope failures were induced by the increasing loads at the slope crest. The interaction of the pipe and the unstable slope is studied to quantify the external forces exerted on the pipe due to the slope failures. Moreover, the influence of a buried pipe on the slope failure mechanism in terms of alterations in the shape of the failure surface is studied.

Physical modelling

Soil characterisation

Two types of sand were used in the tests of this study. The first one is the coarse grained, Merwede river Sand from the Netherlands, which is also known as the Delft Centrifuge Sand (DC Sand), and the second one is the fine Geba Sand. The geotechnical characteristics of these two sands are reported in Table 2. Direct shear tests with three normal stresses of 15.1 kPa, 31.0 kPa and 47.1 kPa were conducted on dense DC Sand samples with relative density of D_r = 75%. Furthermore, consolidated - drained triaxial tests at two different confining pressures of 25 and 100 kPa were performed on Geba Sand samples with relative density of 55% to determine the internal friction angle. The grains of both sands are characterised as sub-angular based on image analysis techniques (De Jager et al. 2017; Maghsoudloo et al. 2017).

Table 3 Summary of relative densities, pipe positions and embedment ratios

Test name	D_r (%)	Pipe position X (m)	Y (m)	H_c/D
NP	70.7	–	–	–
P1	70.6	2.4	1.8	2.96
P2	69.4	2.4	1.2	1.85
P3	69.8	2.4	2.4	4.07
P4	70.0	3.6	1.8	2.22
P5	71.5	4.8	1.8	1.48
NPG	43.6	–	–	–
P1G	43.4	2.9	2.6	4.11

Centrifuge test set-up

The tests were performed using the beam geotechnical centrifuge at TU Delft, which has an arm radius of 1.22 m and is capable of creating an acceleration field of 300 times the Earth's gravity (300 g) with maximum payload of 30 kg (Allersma 1994; Askarinejad et al. 2017). A strongbox was designed with two transparent Plexiglas walls, in order to monitor the movements of the sand grains and the pipe assuming a plane strain condition (Fig. 2). The strain field of the slope as well as the movements of the pipe during the loading on the slope crest were monitored using an advanced high-resolution digital camera facing the transparent side of the model. The images were analysed using particle image velocimetry (PIV) technique (White et al. 2003; Stanier et al. 2015; Askarinejad et al. 2014). All tests were conducted at a centrifugal acceleration field of 30 g.

Model preparation

The samples were prepared using dry pluviation technique (Presti et al. 1992; Pozo et al. 2016) in four steps:

1. Sand layers were poured into the strongbox up to the pipe position level.
2. The pipe was placed carefully on the sand bed.
3. The sand pluviation was resumed to form a flat horizontal layer up to the crest level of the eventual slope.
4. Thin layers of sand were carefully excavated from the model to form the slopes.>

The sand falling height during the dry pluviation was kept fixed at 160 mm above the sand surface. The diffuser ratios

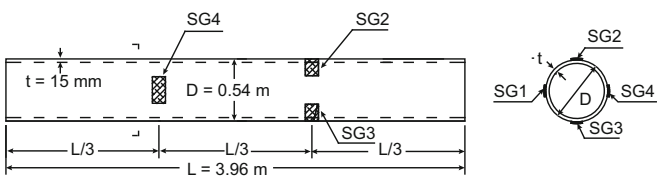

Fig. 3 Dimensions of the pipe in prototype scale and location of the strain gauges

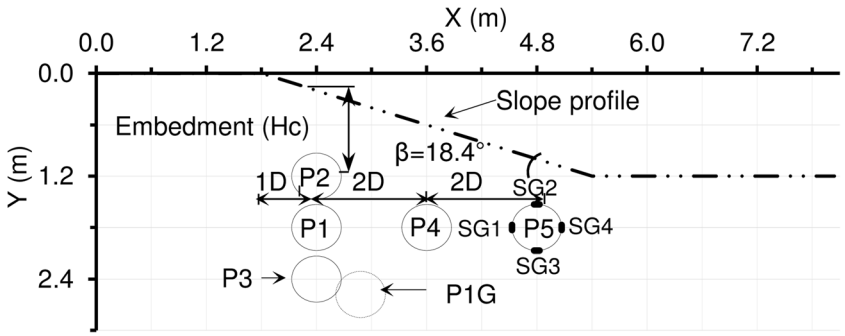

Fig. 4 Five pipe locations for DC Sand tests (P1 to P5) and one pipe location for Geba Sand test (P1G)

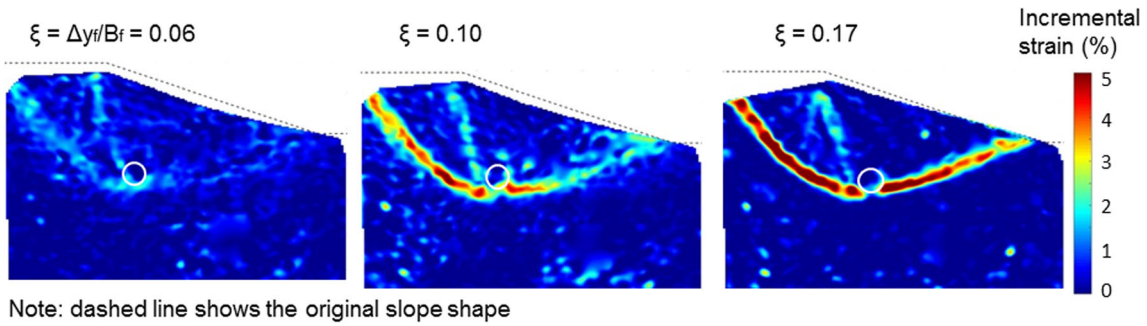

Fig. 5 Incremental shear strain plots for test P1 at three successive normalised footing settlements

(nozzle diameter/D_{50}) for DC Sand and Geba Sand samples were 6.0 and 25.4, respectively. The variation in the attained relative densities of the samples was very low and the average relative densities for the DC and Geba Sand samples were 71% and 43%, respectively. The final slopes have a length of 3.6 m (prototype scale) and angle of 18.7°.

Slope instabilities were induced by pushing a rigid footing onto the slope crests. The footing was connected to the displacement-controlled actuator using a rigid loading rod. A load cell with the capacity of 5 kN (equivalent to 4.5 MN in prototype scale) was installed between the loading rod and the footing.

The dimensions of the pipe have been selected based on three criteria: (1) D/D_{50} ratio, (2) the typical diameter and thickness of the gas pipes in practice and (3) the dimensions of the strong box of the centrifuge. Accordingly, a hollow steel pipe (Young's modulus $E = 193$ GPa) with the outer diameter of $D = 18$ mm (54 mm in prototype scale); wall thickness of $t = 0.5$ mm (15 mm in prototype scale) and length of $L = 132$ mm (3.96 m in prototype scale) was used as the model pipe in these tests (Fig. 3).

The model pipe dimensions have been selected based on typical gas pipes in practice (e.g. Folga 2007). Since the pipe dimensions including the thickness are scaled down by a factor of N as shown in Table 1, and the same material is used for the model pipe as the one in prototype, the scaling factor of pipe flexural rigidity is also satisfied (Taylor 1995). Moreover, this ensures that the outer strain of pipe cross-section in model scale is equal to that in prototype scale.

Ovesen (1981) investigated the uplift capacity of anchor slabs in dry sand by conducting both centrifuge and field tests. While

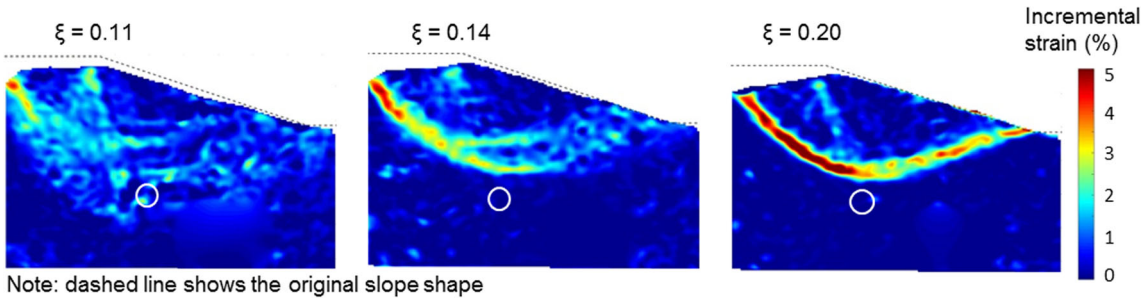

Fig. 6 Incremental shear strain plots of test P3 at three successive normalised footing settlements

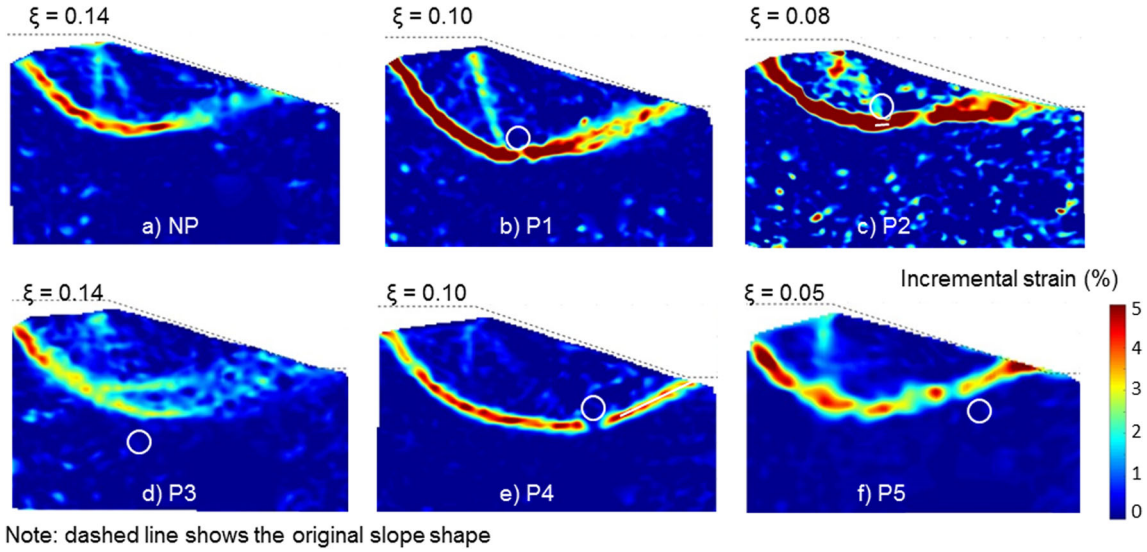

Fig. 7 Failure surfaces of various models at peak bearing capacities of footing

varying the B/D_{50} ratio, where B is the width of the anchor slab, no scale error was observed if $B/D_{50} = 25$ in the centrifuge tests. Considering the analogy between an anchor slab and a pipe as suggested by Garnier et al. (2007) and the fact that the value of D/D_{50} for DC sand is about 20, the particle size effect is evaluated to be minor or negligible in the tests of this study. Four strain gauges (SGs) of type FLA-1-350-11 were installed at 90° angles on the pipe to monitor the cross-section deformations caused by the external forces during the slope instabilities.

Testing programme

In total, eight tests were conducted on sandy slopes with and without buried pipes (Table 3). Six tests were performed on sample slopes built with DC Sand (NP, P1 to P5) and the other two were made on slopes with Geba Sand (NPG and P1G). While the geometry of all slopes is identical, the position of the pipes has been altered over five locations (P1 to P5). The geometry of the slopes in prototype scale and the locations of the pipes are shown in Fig. 4. For clarity, all tests were named based on the pipe positions. *Pi* represents the pipe at location *i*, where $i = 1$ to 5 (as shown in Fig. 4 and summarised in Table 3), while NP is the test without a pipe. The added letter *G* to the last two tests refers to the Geba Sand tests. All tests were repeated at least once to check the reproducibility of the results.

Pipe locations were designed based on the shape and location of the failure surface in the samples without a pipe, which is regarded as the potential failure surface (PFS). The displacements and the shear strains of the samples as well as the exact location of the failure surfaces were obtained using PIV method. For the DC Sand tests, firstly, the test without the pipe (NP) was conducted aiming to investigate the location of PFS. Thereafter, five pipe locations (Fig. 4) were selected to measure the loads applied to the pipes and to explore the effect of the pipes on the shape of the failure surface. Accordingly, P1 was placed at the deepest point of PFS, whereas, P2 and P3 were approximately 1*D* (one pipe diameter) above and below P1, respectively. P4 and P5 were approximately 2*D* and 4*D* further away from P1 towards the slope toe, respectively.

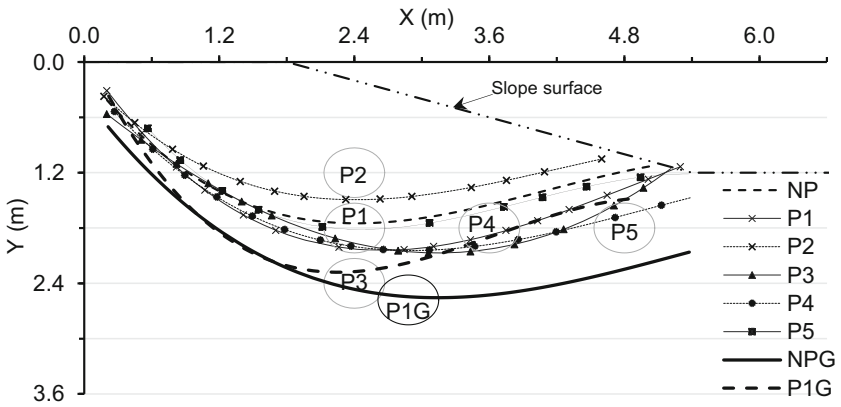

Fig. 8 Failure surfaces of both DC Sand samples and Geba Sand samples

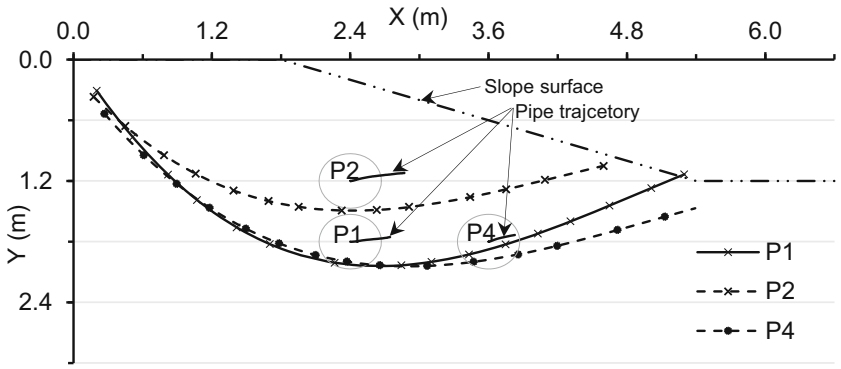

Fig. 9 Trajectories of P1, P2 and P4

Results and discussion

Failure mechanisms

Incremental shear strain plots at three successive normalised footing settlements (ξ) of tests P1 and P3 are shown in Figs. 5 and 6, respectively. The factor ξ indicates the ratio between the footing settlement (Δy_f) and the footing width (B_f). The incremental shear strain plot is the shear strain map obtained from two successive captured images during the loading process, and illustrates the location of the shear band in the slope. Figure 7 shows all of the incremental shear strain plots for DC Sand samples when the corresponding failure surfaces were fully formed.

Figures 5 and 6 indicate that the shear strains initiated at the edges of the footing and extended towards the pipe at the early stages of the loading. With increasing ξ, a shear band became more noticeable. The slope failure happened when the value of ξ reached about 0.10. It is obvious that the failure surface of test P1 (FS_P1) passes below the pipe and the same phenomenon can be observed in tests P2 and P4 (Fig. 7). The failure surfaces of both tests P3 (Fig. 6, FS_P3) and P5 (Fig. 7, FS_P5) were above the pipes, which are the deepest and farthest pipe positions with respect to the crest. These observations imply that only if the pipe is placed at a location close enough to the potential failure surface can the failure surface pass below the pipe.

All failure surfaces are summarised in Fig. 8. By taking PFS as a benchmark, it is notable that the existence of the pipes influenced the propagation of the failure surfaces. Results of the tests in which the pipes were horizontally placed at about 1*D* distance to the crest edge (P2, P1 and P3) show that a deeper pipe resulted in a deeper failure surface. Failure surfaces in tests P1 and P2 formed beneath their respective pipes. Hence, the pipe can be regarded as a weak zone in each sample. There are two reasons: first, the hollow pipe is lighter than the soil mass with the same volume; second, the sand-pipe interface is smoother than the sand-sand interface. For the test P3, though FS_P3 did not form below the pipe, it was deeper than FS_P1. As P3 was about 1*D* deeper than PFS and had the highest confining stress condition, it moved the least (further shown in Fig. 10). However, the amount of soil mass just above the crown of P3 was easier to deform compared with the soil at the same place of test NP. This explains the fact that the first half of FS_P3 was steeper than that of PFS (Fig. 8).

Similarly, results of the tests in which the pipes were positioned at the same horizontal level (P1, P4 and P5) illustrate that the influence of the pipes on the failure surfaces was getting less

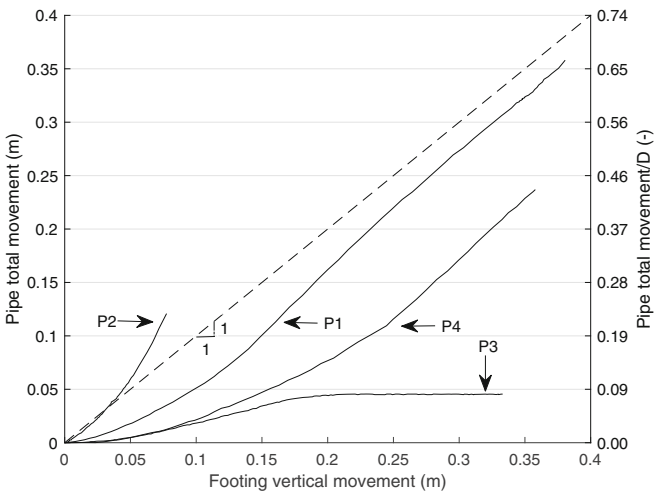

Fig. 10 Total pipe movement with respect to footing vertical movement in prototype scale

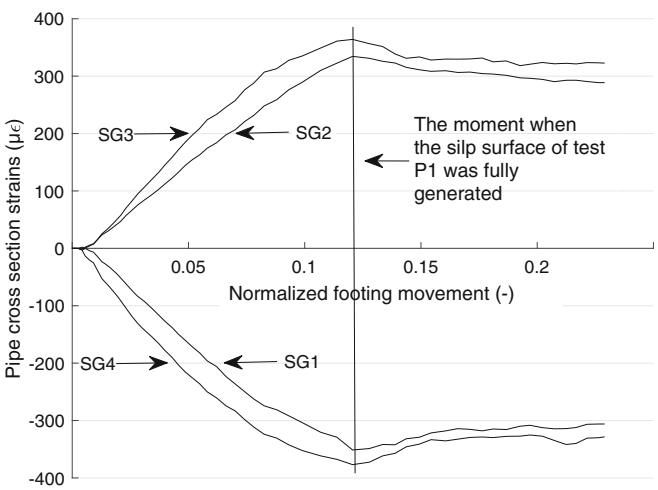

Fig. 11 Development of the cross section strains of P1

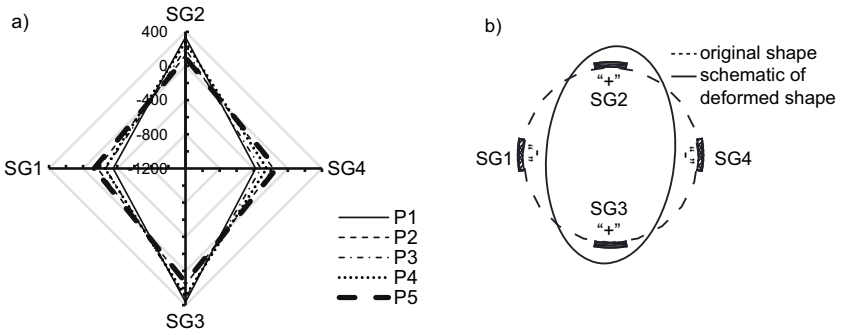

Fig. 12 **a**) Maximum pipe strain measurements tests with DC Sand; **b**) schematic deformation of the pipe cross-section caused by the slope failure

significant with increasing burial distance to the slope crest. The failure surface of P4 ended further than FS_P1, as P4 was buried further than P1. It is observed that FS_P5 was very close to PFS (Fig. 8,) which indicates that P5 hardly affected the slope failure. This might be due to the fact that it was the closest pipe to the slope toe and also lower than PFS. Comparing the effects of pipes on the failure mechanisms, it can be inferred that if a pipe is buried no more than 0.5D below PFS, the failure surface tends to pass below the pipe.

Comparing the test NPG with the test NP, the failure surface location of NPG is generally lower than that of NP (Fig. 8). Furthermore, the failure surface of P1G developed above the pipe when the pipe was placed at the lowest point of the failure surface of NPG. This is a different behaviour compared to the test P1 but is similar to the test P3. P1G was close to but lower than P3 and had a larger value of H_c/D ratio than that of P3 which might result in the failure surface passing above P1G.

Pipe movement

It can be assumed that the friction between the pipe ends and the strong box walls is less than that between the sand grains and the side walls. Furthermore, to prevent ingress of sand particles, the two ends of the pipe were carefully covered with thin lubricated layers of plastic. Hence, the friction between the strong box wall and the pipe is considered to be insignificant. Markers were made on the pipe end cover, which was facing the camera in order to track the pipe movement using PIV method.

The traces of P1, P2 and P4 are demonstrated in Fig. 9. It can be seen that each pipe moved along failure surface in each slope instability test. Furthermore, the magnitude of pipe movement decreases as the distance to the slope crest increases. Figure 10 illustrates the total movements of the pipes with respect to the footing vertical movement. Comparing the behaviour of P1, P2 and P3, the shallower pipes had relatively larger movements. P2 had the largest pipe displacement, since it had the shallowest burial depth and the shallowest failure surface. The movements of P1 and P4 demonstrate a decreasing trend as the original location of the pipe moved towards the toe. The moving rate of P2 was slightly higher than that of the footing, while the moving rates of P1 and P4 after their corresponding failures were comparable with the footing settlement rate.

Cross-section deformation of the pipes

The deformed shape of pipe cross-section can be inferred from the measurements of the four strain gauges secured on the pipe as shown in Fig. 3. All tests had the same pattern of strain development. Results of P1 are illustrated in Fig. 11. The four SGs reached their peak values at the same moment when the failure surface was fully generated.

The strain measurements before loading were subtracted from total strain measurements. Hence, the initial deformation due to the soil weight was excluded. The peak strain measurements of the pipes for different tests and the schematic deformed shape of the pipe are plotted in Fig. 12. Based on the maximum pipe cross-section strain measurements, it can be inferred that the pipe deformation of each test was symmetric since the peak values of the opposite strain gauges were almost identical (Fig. 12a). The maximum average value of SG2 and SG3 as well as that of SG1 and SG4 for each test are summarised in Table 4 and are used to calculate the external forces on the pipe in the following section. Note that positive value stands for extension.

Table 4 Estimated ultimate acting forces on the pipes and their respective directions

Test	$\frac{\varepsilon_{1,\max}+\varepsilon_{4,\max}}{2}$ ($\mu\varepsilon$)	$\frac{\varepsilon_{2,\max}+\varepsilon_{3,\max}}{2}$ ($\mu\varepsilon$)	The ultimate acting force, F_{uN} (kN/m)	F_{uN} direction, θ_u (°)
P1	− 364.69	349.30	59.52	17.94
P2	− 127.21	104.30	16.55	12.98
P3	− 288.12	259.74	43.05	16.08
P4	− 251.57	286.07	53.58	22.63
P5	− 129.91	115.51	18.99	15.64
P1G	− 372.13	374.60	65.47	19.39

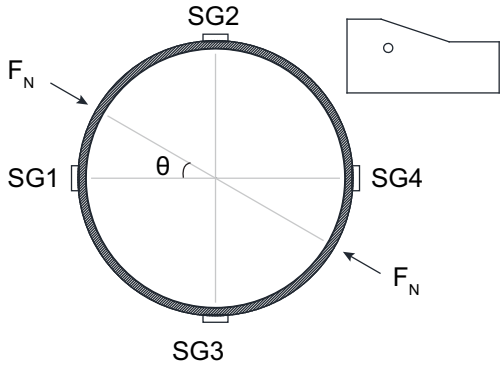

Fig. 13 Simplified model of acting forces on a pipe embedded inside an unstable slope

External forces on the pipes

The external forces acting on the pipe during the soil movements can be simplified as a pair of dominant counterbalancing point forces (F_N) as depicted in Fig. 13. The outer strain (ε) for an arbitrary point of the pipe with an angle of θ with respect to the direction of the counterbalancing point forces has the following relationship with the magnitude of the acting force F_N:

$$-\varepsilon = \frac{6F_N\, r}{Et^2}\left(\frac{1}{\pi} - \frac{|sin\theta|}{2}\right) \tag{4}$$

where r is the outer radius, E is the Young's modulus of the pipe material and t is the wall thickness of the pipe. Note that F_N is in the unit of kN/m. Hence, the four cross-section stain measurements (ε_i) can be expressed in Eq. (5).

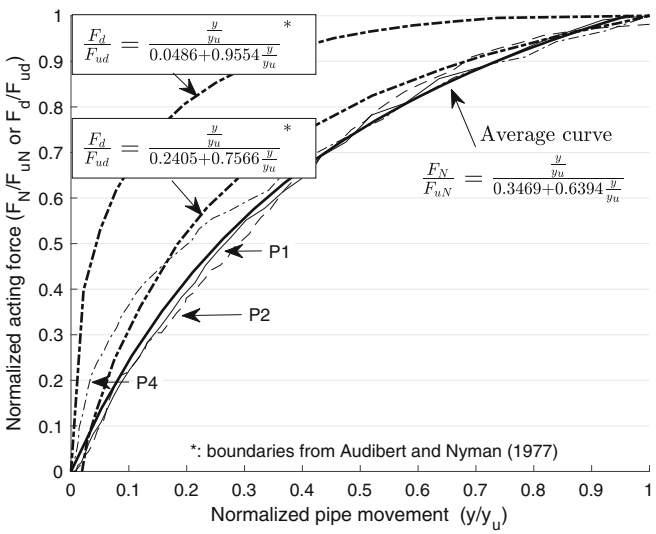

Fig. 14 Normalised acting force vs. normalised pipe movement

Table 5 Ratios of ultimate pipe movements with respect to pipe-embedment depths

	P1	P2	P4
y_u/H_c	0.09	0.12	0.08

$$\begin{cases} -\varepsilon_3 = -\varepsilon_2 = \dfrac{6F_N\, r}{Et^2}\left(\dfrac{1}{\pi} - \dfrac{\cos\theta}{2}\right) \\ -\varepsilon_1 = -\varepsilon_4 = \dfrac{6F_N\, r}{Et^2}\left(\dfrac{1}{\pi} - \dfrac{\sin\theta}{2}\right) \end{cases} \tag{5}$$

By solving Eq. (5) with the maximum strain measurements, i.e. $\varepsilon_{1,\,max}$ and $\varepsilon_{3,\,max}$, the ultimate values of point load (F_{uN}) and it is direction (θ_u) can be determined from Eq. (6) and Eq. (7), respectively. Equation (6) has two answers; however, F_{uN} should be a positive value because the acting forces due to the slope instability should be compressing the pipe. The maximum acting forces and the respective directions with respect to horizontal are represented in Table 4. Note that, since the initial strains due to soil weight have been subtracted, F_{uN} in Table 4 was induced only by the slope failure.

$$F_{uN} = -\frac{\pi Et^2}{3r}\frac{\left(\varepsilon_{3,max}^2 + \varepsilon_{1,max}^2\right)}{\left(2\varepsilon_{1,max} + 2\varepsilon_{3,max} \pm \pi\sqrt{\varepsilon_{3,max}^2 - \left(\frac{2}{\pi}\left(\varepsilon_{3,max} - \varepsilon_{1,max}\right)\right)^2 + \varepsilon_{1,max}^2}\right)} \tag{6}$$

$$\theta_u = \sin^{-1}\frac{\frac{2}{\pi}\left(\varepsilon_{3,max} - \varepsilon_{1,max}\right)\varepsilon_{3,max} \mp \varepsilon_{1,max}\sqrt{\varepsilon_{3,max}^2 - \left(\frac{2}{\pi}\left(\varepsilon_{1,max} - \varepsilon_{3,max}\right)\right)^2 + \varepsilon_{1,max}^2}}{\left(\varepsilon_{3,max}^2 + \varepsilon_{1,max}^2\right)} \tag{7}$$

Audibert and Nyman (1977) found the normalised force-pipe movement relationships of their results were hyperbolic and were bounded by two curves. The normalised test results are compared with these two boundaries in Fig. 14. The test results follow hyperbolic trend but are slightly below the lower boundary suggested by Audibert and Nyman (1977). This might be attributed to the difference between the two testing environments, i.e. level ground and sloping ground. The two constant values, a and b, in Eq. (2), were obtained by fitting the test results. The average curve and corresponding function are shown in Fig. 14. Only the results of tests P1, P2 and P4 are discussed here and after, because the pipes of other tests were not in the corresponding sliding zones.

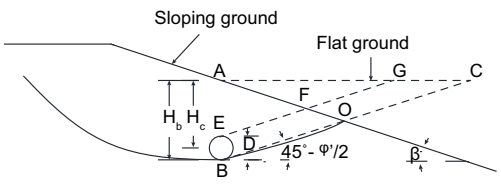

Fig. 15 Slip surface of a slope with a buried pipe

Table 6 Values of ω for tests P1, P2 and P4

	H_c (m)	L_c (m)	ω
P1	1.6	0.6	0.594
P2	1.0	0.6	0.330
P4	1.2	1.8	0.759

The values of y_u/H_c are summarised in Table 5. The results of the tests P1 and P4 are in good agreement with the estimation by Trautmann and O'Rourke (1985) for medium dense sand. Nevertheless, y_u/H_c for test P2 is comparable with the estimation for loose sand.

Estimation of the ultimate acting forces on pipelines in slopes

The results of the centrifuge tests are used in this chapter to derive a general formulation to determine the normal load applied to a pipe in an unstable slope. The maximum soil load acting on a pipe buried in a flat ground surface depends on the soil unit weight, pipe-embedment depth and the ultimate bearing capacity factor, which is a function of H_c/D and soil friction angle (Trautmann and O'Rourke 1985, Guo and Stolle 2005). This dependency is generally presented using Eq. (1). However, the ultimate soil force acting on a pipe in the sloping ground condition (q_{us}) depends not only on the soil unit weight, pipe-embedment depth and ultimate bearing capacity factor but also depends on the location of the pipe centre with respect to the slope crest (L_c) as well as on the slope angle (β). The parameter L_c is specifically important for the case of a rotational slope failure mechanism. The effect of slope angle on the ultimate soil load on the pipe is investigated in the following section, and thereafter, a general equation is derived to account the impact of other factors on the load transferred from the moving soil to the pipe.

Effect of slope angle on the applied force to the pipe

Audibert and Nyman (1977) proposed Eq. (1) for pipes buried under the flat ground condition; however, this equation cannot be directly applied to a pipe buried in a slope due to the geometric difference

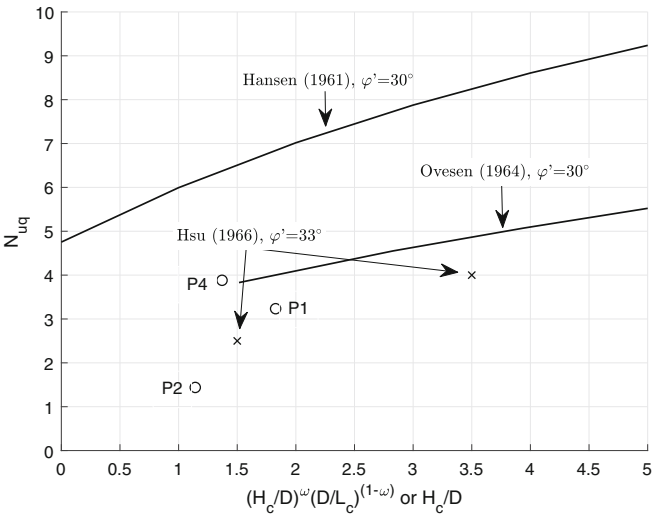

Fig. 16 Comparison between measured N_{uqs} and N_{uq} estimated from three previously published methods

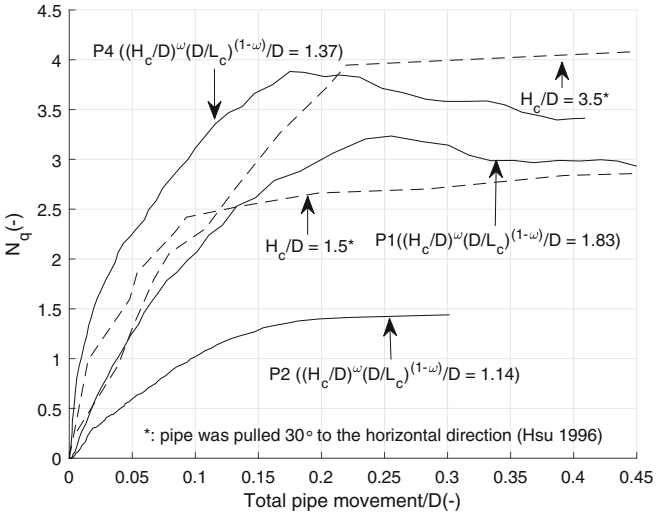

Fig. 17 Development of dimensionless force on pipe with pipe movement

between the two ground surface conditions as shown in Fig. 15. Line AO is the slope surface, line AC is the hypothetical level ground, and line BO has an inclination of $45°-\phi'/2$ suggested by Hansen (1961), where ϕ' is the internal soil friction angle of the soil.

In order to link the ultimate soil resistance for the sloping ground condition, q_{us}, with the ultimate soil resistance for the flat ground condition, q_u, a geometric factor α is introduced in this study. The factor α can also be regarded as the ultimate soil resistance ratio between the two ground surface conditions as expressed by Eq. (8). The geometric factor α is approximated by the ratio between the areas of EBOF and EBCG, i.e. S_{EBOF}/S_{EBCG}, as shown in Eq. (9), which is dependent on the soil friction angle and the slope angle.

$$q_{us} = \alpha q_u \tag{8}$$

$$\alpha = \frac{S_{EBOF}}{S_{EBCG}} = \frac{\tan\left(45^\circ - \phi'/2\right)}{\tan\beta + \tan\left(45^\circ - \phi'/2\right)} \tag{9}$$

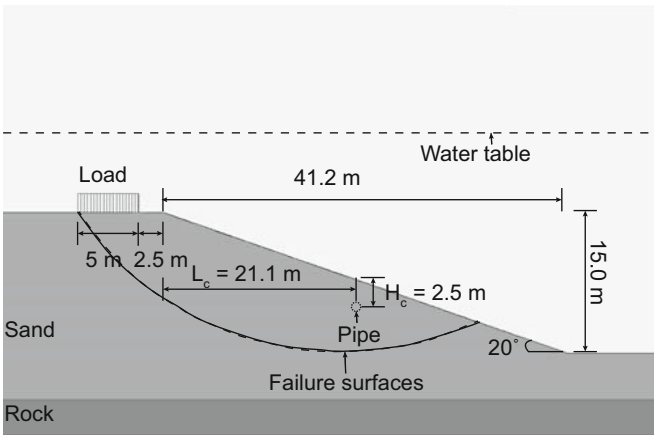

Fig. 18 A case study of slope instability

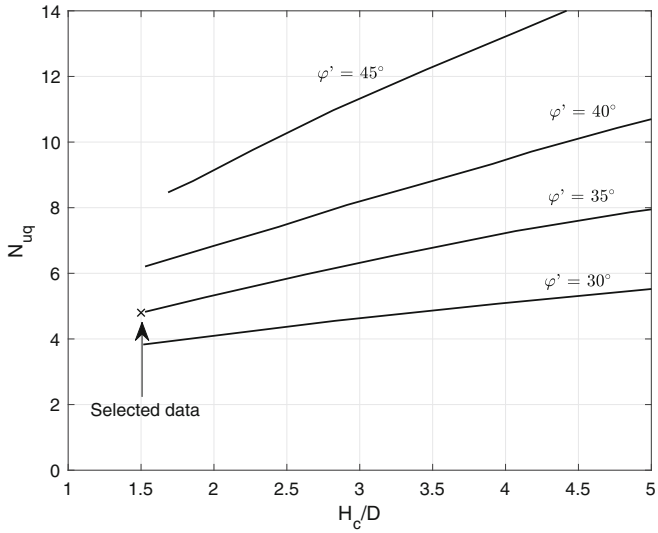

Fig. 19 Plot of N_{uq} versus H_c/D modified from Ovesen (1964)

It should be noted that during the process of slope failure, the pipe position and the slope surface (AO in Fig. 15) are changing; however, these changes are assumed to be negligible at small soil strains.

Effect of buried depth and buried distance to the slope crest on the applied force to the pipe

Equation (10) is proposed to accommodate the dependencies of the burial depth (H_c) and the distance to the slope crest (L_c). The model parameter ω is a weight factor indicating the influence of H_c compared with the influence of L_c on q_{us}. Substituting Eqs. (1) and (9) into Eq. (10) yields the model parameter ω to be defined as demonstrated in Eq. (11). When the pipe is buried under a flat surface, geometric factor α is 1 (see Eq. (9)) and yields ω to be 1; hence, Eq. (10) reduces to Eq. (1). In this study, the slope angle (β) is 18.4° and ϕ' is 33.6°; hence, α equals to 0.62. The values of ω for P1, P2 and P4 can be obtained from Eq. (11) and are listed in Table 6.

$$q_{us} = \gamma D \left(\frac{H_c}{D}\right)^{\omega} \left(\frac{D}{L_c}\right)^{1-\omega} N_{uq} \tag{10}$$

$$\omega = 1 + \frac{\ln\alpha}{\ln(L_c/D) + \ln(H_c/D)} \tag{11}$$

The values of N_{uq} for tests P1, P2 and P4 are shown in Fig. 16 with respect to the newly defined embedment ratio ($(\frac{H_c}{D})^{\omega}(\frac{D}{L_c})^{1-\omega}$). Results show a very good agreement with N_{uq} predicted by Ovesen (1964), Hansen (1961) and Hsu (1996).

Figure 17 illustrates N_{qs} versus normalised pipe movement for P1, P2 and P4. The results show that N_{qs} increased with the pipe movement and reached their ultimate values. After reaching peaks, N_{qs} fell down slightly (P1 and P4) or stayed constant (P2). It is also remarkable that a deeper sliding surface (see Fig. 8) resulted in a higher stiffness for the normalised force-pipe movement curve. Furthermore, the development of N_{qs} with raising pipe movement generally follows the observations of Hsu (1996) as demonstrated in Fig. 17.

Application of results

For illustrating the estimation of the ultimate soil load acting on a pipe, a sandy slope with the dimensions shown in Fig. 18 is considered. Two scenarios of dry and fully submerged slopes are simulated. The soil is composed of medium dense sand with a friction angle of 35°, the dry and saturated unit weights are 18 and 20 kN/m^3, respectively. The sand layer is deposited above the bedrock layer in both cases. The slope instability is triggered by loading the slope crest. The slope instability analysis is conducted based the Bishop's method of slices (Bishop and Morgenstern 1960) using D-Geo Stability software (version 16.2), and gives a potential failure surface as illustrated in Fig. 18.

A 1.0-m diameter gas pipe is buried in the slope above the potential failure surface as illustrated in Fig. 18. The ultimate soil load applied to the pipe can be calculated using the following steps:

Step 1 Calculation of the geometric factor α. Equation (9) leads to a value of 0.589 for α when $\beta = 20^{\circ}$ and $\phi' = 35^{\circ}$.

Step 2 Calculation of the parameter ω from Eq. (11). H_c/D is 2.5 and L_c/D is 21.1 and these parameters result ω to be 0.867.

Step 3 Calculation of the value N_{uq} from the method proposed by Ovesen (1964) based on the newly defined embedment ratio ($(\frac{H_c}{D})^{\omega}(\frac{D}{L_c})^{1-\omega} = 1.5$). Figure 19 shows N_{uq} from the method of Ovesen (1964), which is applicable for both dry and saturated conditions. Hence, a value of 4.8 is selected for N_{uq} as indicated in Fig. 19.

Step 4 Calculation of q_{us}. The values of ultimate soil load on the pipe in two scenarios of dry and submarine slopes are calculated using Eq. (10). $q_{us} = 127.2$ kPa and $q_{us} = 70.7$ kPa are obtained for the dry and submerged slopes, respectively.

Summary and conclusions

In this paper, the behaviour of buried pipes in unstable sandy slopes was studied by means of centrifuge modelling. The magnitudes of the induced external forces to the pipe due to slope instability were investigated and the influence of the pipes on the development of the failure surfaces were discussed. The forces acting on the pipes buried in sloping grounds were compared with published results based on the tests on pipes under flat surfaces. Moreover, the effect of the pipe burial distance to the slope crest on the bearing capacity factor was illustrated. In addition, a geometric factor was introduced to modify the bearing capacity factor suggested for pipes buried in flat grounds. The following conclusions can be derived based on the conditions that the embedment ratio of a pipe is less than or equal to 4.1 in a sandy sloping ground subjected to surcharge loading:

1. Pipes buried within the potential failure zones of the slopes suffer larger movements than those buried outside the potential failure surfaces. The potential failure surface can be estimated using analytical or numerical methods, such as the limit equilibrium or finite element methods in the process of the design or evaluating a segment of a pipeline in a slope cross-section.
2. The failure surface tends to pass below the pipe when it is placed no more than 0.5D below the potential slip surface.
3. The bearing capacity factors for pipes buried in slopes should be dependent not only on the soil unit weight, pipe diameter and burial depth but also on the slope angle and the pipe burial distance to the slope crest.

4. The normalised force-pipe displacement relationship could be represented by a hyperbolic equation.>

The maximum external force exerted on the pipe due to any circular failure mechanism of the slope can be predicated based on the method presented in this study. For the condition that the pipe is not located inside the failure zone, the proposed method for estimating the ultimate dimensionless force is invalid. However, in this case, the centrifuge tests' results of this study indicate that there is no necessity to consider the maximum pipe external forces induced by a landslide, as the pipe will be hardly influenced. Nevertheless, further investigations with other slope angles and more pipe positions are necessary to validate the proposed method.

Acknowledgements

The first author was supported by China Scholarship Council. The writers are thankful to Andrew Zi-Xiang Gng, Johan Schuringa, J.J. de Visser, Kees van Beek and Ronald van Leeuwen for assistance with the experimental work.

References

Allersma HGB (1994) The University of Delft geotechnical centrifuge. Int. Conf. Centrifuge 94, 31 August-2 Sept 1994 Balkema, Rotterdam. 47–52

Almahakeri M, Fam A, Moore ID (2013) Experimental investigation of longitudinal bending of buried steel pipes pulled through dense sand. J Pipeline Syst Eng Pract 5:04013014

Askarinejad A, Beck A, Springman SM (2014) Scaling law of static liquefaction mechanism in geocentrifuge and corresponding hydromechanical characterization of an unsaturated silty sand having a viscous pore fluid. Can Geotech J 52:708–720

Askarinejad A, Philia Boru Sitanggang A, Schenkeveld F (2017) Effect of pore fluid on the behavior of laterally loaded offshore piles modelled in centrifuge. 19th International Conference on Soil Mechanics and Geotechnical Engineering (ICSMGE 2017), 2017 Seoul. 897–900

Audibert JM, Nyman KJ (1977) Soil restraint against horizontal motion of pipes. J Geotech Eng Div 103:1119–1142

Bishop AW, Morgenstern NR (1960) Stability coefficients for earth slopes. Géotechnique 10:164–169

Calvetti F, Di Prisco C, Nova R (2004) Experimental and numerical analysis of soil–pipe interaction. J Geotech Geoenviron 130:1292–1299

Chan PDS, Wong RCK (2004) Performance evaluation of a buried steel pipe in a moving slope: a case study. Can Geotech J 41:894–907

De Jager RR, Maghsoudloo A, Askarinejad A and Molenkamp F (2017) Preliminary results of instrumented laboratory flow slides. *1st International Conference on the Material Point Method*. Delft, The Netherlands: Elsevier Ltd.

Di Prisco C, Galli A (2006) Soil-pipe interaction under monotonic and cyclic loads: experimental and numerical modelling. Proceedings of the First EuroMediterranean Symposium in Advances on Geomaterials and Structures, 2006 Hammamet, Tunisia 755-760

Feng W, Huang R, Liu J, Xu X, Luo M (2015) Large-scale field trial to explore landslide and pipeline interaction. Soils Found 55:1466–1473

Folga S (2007) Natural gas pipeline technology overview. United States: Argonne National Lab. (ANL), Argonne, IL

Garnier J, Gaudin C, Springman SM, Culligan PJ, Goodings DJ, Konig D, Kutter B, Phillips R, Randolph R, Thorel L (2007) Catalogue of scaling laws and similitude questions in geotechnical centrifuge modelling. Int J Phys Model Geotech 8:1–23

Guo P, Stolle D (2005) Lateral pipe–soil interaction in sand with reference to scale effect. J Geotech Geoenviron 131:338–349

Hansen JB (1961) The ultimate resistance of rigid piles against transversal forces. Bulletin 12:5–9

Hsu T-W (1996) Soil restraint against oblique motion of pipelines in sand. Can Geotech J 33:180–188

Liu R, Guo S, Yan S (2015) Study on the lateral soil resistance acting on the buried pipeline. J Coast Res 73:391–398

Maghsoudloo A, Galavi V, Hicks M, Askarinejad A (2017) Finite element simulation of static liquefaction of submerged sand slopes using a multilaminate model. *19th International Conference on Soil Mechanics and Geotechnical Engineering*. Seoul

Nyman KJ (1984) Soil response against oblique motion of pipes. J Transp Eng 110:190–202

Oliveira JR, Almeida MS, Almeida MC, Borges RG (2009) Physical modeling of lateral clay-pipe interaction. J Geotech Geoenviron 136:950–956

Oliveira JRM, Rammah KI, Trejo PC, Almeida MS, Almeida MC (2017) Modelling of a pipeline subjected to soil mass movements. Int J Phys Model Geotech 17:246–256

Ono K, Yokota Y, Sawada Y, Kawabata T (2017) Lateral force–displacement prediction for buried pipe under different effective stress condition. Int J Geotech Eng 1–9

Ovesen NK (1964) Anchor slabs: calculation methods and model tests. Bulletin 16, 1964 Copenhagen. Danish Geotechnical Institute

Ovesen NK (1981) Centrifuge tests of uplift capacity of anchors. Proceedings of the 10th international conference on soil mechanics and foundation engineering, 1981 Stockholm. 717-722

Paulin MJ (1998) An investigation into pipelines subjected to lateral soil loading. Doctoral dissertation, Memorial University of Newfoundland

Pozo C, Gng Z, Askarinejad A (2016) Evaluation of Soft Boundary Effects (SBE) on the Behaviour of a Shallow Foundation. 3rd European Conference on Physical Modelling in Geotechnics (EUROFUGE 2016), 2016 France: Nantes. 385–390

Presti DCL, Pedroni S, Crippa V (1992) Maximum dry density of cohesionless soils by pluviation and by ASTM D 4253-83: a comparative study. Geotech Test J 15:180–189

Rammah KI, Oliveira JR, Almeida MC, Almeida MS, Borges RG (2014) Centrifuge modelling of a buried pipeline below an embankment. Int J Phys Model Geotech 14:116–127

Roy KS, Hawlader B (2012) Soil restraint against lateral and oblique motion of pipes buried in dense sand. 2012 9th international pipeline conference, September 24–28 2012 Calgary. Calgary, Alberta, Canada: American Society of Mechanical Engineers, 7–12

Sahdi F, Gaudin C, White D, Boylan N, Randolph M (2014) Centrifuge modelling of active slide-pipeline loading in soft clay. Géotechnique 64:16–27

Schofield AN (1980) Cambridge geotechnical centrifuge operations. Géotechnique 30:227–268

Stanier SA, Blaber J, Take WA, White DJ (2015) Improved image-based deformation measurement for geotechnical applications. Can Geotech J 53(5):727–739

Taylor RN (1995) Geotechnical centrifuge technology. Blackie Academic & Professional, Glasgow

Terzaghi K (1943) Theoretical soil mechanics. Wiley Publications, New York

Tian Y, Cassidy MJ (2011) Pipe-soil interaction model incorporating large lateral displacements in calcareous sand. J Geotech Geoenviron 137:279–287

Trautmann CH, O'rourke TD (1985) Lateral force-displacement response of buried pipe. J Geotech Eng 111:1077–1092

White D, Take W, Bolton M (2003) Soil deformation measurement using particle image velocimetry (PIV) and photogrammetry. Geotechnique 53:619–631

Wood DM (2003) Geotechnical modelling. CRC Press, Boca Raton

Wu J, Zhou R, Xu S, Wu Z (2017) Probabilistic analysis of natural gas pipeline network accident based on Bayesian network. J Loss Prev Process Ind 46:126–136

Yimsiri S, Soga K, Yoshizaki K, Dasari G, O'rourke T (2004) Lateral and upward soil-pipeline interactions in sand for deep embedment conditions. J Geotech Geoenviron 130:830–842

Zhang J, Stewart DP, Randolph MF (2002) Modeling of shallowly embedded offshore pipelines in calcareous sand. J Geotech Geoenviron 128:363–371

W. Zhang · A. Askarinejad (✉)
Faculty of Civil Engineering and Geosciences,
TU Delft,
Delft, The Netherlands
Email: A.Askarinejad@tudelft.nl

W. Zhang
e-mail: w.zhang-3@tudelft.nl